Journal of Applied Physics ARTICLE scitation.org/journal/jap

Harnessing rainbow trapping via hybrid electromechanical metastructures for enhanced energy harvesting and vibration attenuation

Cite as: J. Appl. Phys. **132**, 064903 (2022); doi: 10.1063/5.0090258
Submitted: 4 March 2022 · Accepted: 17 July 2022 ·
Published Online: 9 August 2022

Jonatha Santini,[1] Christopher Sugino,[2] Emanuele Riva,[1,a)] and Alper Erturk[3]

AFFILIATIONS

[1]Department of Mechanical Engineering, Politecnico di Milano, Via La Masa 1, Milano 20156, Italy
[2]Department of Mechanical Engineering, Stevens Institute of Technology, Hoboken, New Jersey 07030, USA
[3]George W. Woodruff School of Mechanical Engineering, Georgia Institute of Technology, Atlanta, Georgia 30332, USA

[a)]**Author to whom correspondence should be addressed:** emanuele.riva@polimi.it

ABSTRACT

Rainbow trapping is a phenomenon that enables vibration confinement due to the gradual variation of the wave velocity in space, which is typically achieved by means of locally resonant unit cells. In the context of electromechanical metastructures for energy harvesting, this strategy is employed to improve mechanical-to-electrical energy conversion and thereby to maximize the harvested power. In contrast to structures endowed with either mechanical or electromechanical resonators, we investigate a hybrid configuration that leverages the synergistic interplay between them. We compare numerical results for different grading laws in comparison to prior efforts on the topic, demonstrating enhanced energy harvesting and wideband vibration attenuation capabilities of the hybrid metastructure. We also discuss the formation of grading-induced localized modes and we shed light on the role of the motion of individual resonators on the overall power output increase.

NOMENCLATURE

b^c	Width of the beam
b^r	Width of the mechanical resonators
$Cp^{c,r}$	Inherent piezoelectric capacitance
c_s	Young's modulus of the beam
$\bar{c}_{11}^E$	Short circuit Young's modulus
c_j	Damping of the jth mechanical resonator
EI	Equivalent flexural rigidity
$\bar{e}_{31}$	Effective piezoelectric stress constant
$h_j^{c,r}$	Normalized admittance across the jth electrode
$h_p^{c,r}$	Thickness of the piezoelectric patch
h_s^c	Substrate thickness of the beam
k_j	Stiffness of the jth mechanical resonator
L	Beam length
L^r	Length of the mechanical resonators
m	Equivalent linear mass density
m_j	mass of the jth mechanical resonator
N	Number of modes assumed
$R_j^{c,r}$	Resistance across the jth electrode
S	Number of resonators
x_j^L	Left edge of the jth electrode
x_j^R	Right edge of the jth electrode
$Y_j^{c,r}$	Admittance across the jth electrode

Greek

$\delta(x)$	Dirac delta function
Δx	Spacing between resonators
γ	Dimensionless coupling term
μ	Mass ratio
ω_k	k^{the} natural frequency of the beam
ω_j^c	Resonant frequency of the jth shunt circuit
ω_j^r	resonance frequency of the jth mechanical resonator
ω_t	Resonators tuning frequency
ρ_p	Density of the piezoelectric layer
ρ_s	Substrate density of the beam
$\theta_j^{c,r}$	Electromechanical coupling for the jth resonator
$\tau_j^{c,r}$	Time constant of the jth shunt circuit
$\bar{\varepsilon}_{33}^S$	Permittivity at constant strain in the expansion
ζ_j	Dimensionless damping for the jth resonator
ζ_k	kth modal damping for the beam

I. INTRODUCTION

The research done in the context of acoustic/elastic metamaterials has sparked broad interest within different realms of engineering, which is motivated by a number of behaviors technologically relevant that are not possible to pursue otherwise. In other words, after the discoveries reported in the early paper of Liu *et al.*,[1] much effort has been devoted to the quest for novel metamaterial concepts in mechanics.

A possible implementation extensively discussed in the past few years consists in a host medium, which is artificially altered through a number of locally resonant units periodically placed in space. In the homogenization limit, such a configuration is known to exhibit effective properties that are dynamically unusual, such as negative mass[2–4] or negative stiffness effects,[5,6] yielding the formation of frequency bandgaps, i.e., modified dispersion bands in which wave propagation occurs with attenuation characteristics. The capability to manipulate elastic waves and vibrations has led to a number of studies paving the application of metamaterials for isolation purposes,[7,8] communication,[9,10] imaging,[11] and enhanced sensing in structures,[12] among others.

Recently, the study of mechanical metamaterials for vibration attenuation purposes has reached a mature state due to the abundance of works reported in the literature, which have set general guidelines to generate low frequency, and broadband attenuation characteristics. As such, more exciting and exotic wave phenomena are to be sought via more complex or multifunctional configurations. Another established yet not mature line of work explores multi-physics interactions to provide new degrees of freedoms in the design of metamaterial systems, especially through piezoelectric actuation. Relevant examples include implementations of nonreciprocal devices,[13–15] selective filters,[16] digitally controllable waveguides,[17,18] among others. Application-wise, there is great interest in piezoelectric-based metamaterials due to the interplay between electrical and mechanical oscillations, which is key to design structures with energy harvesting capabilities.[19] In analogy with purely passive metamaterials, in which the attenuation features are due to energy storage through the resonator motion, electromechanical metamaterials can be implemented through periodic patterns of piezoelectric elements bonded on otherwise passive structures and equipped with electrical circuits that serve as a means to induce resonant interactions with the host structure.[6] The underlying physics naturally yields concurrent wave attenuation (bandgap formation) and energy harvesting features when suitable conversion circuits are considered.[20]

Additional opportunities in this context are offered by *graded metastructures*, i.e., a relatively new family of metastructures in which the dynamic characteristics of the locally resonant units are smoothly modulated in space, thereby inducing the so called *rainbow effect*. Graded metamaterials have been recently investigated within different realms of physics and by way of different physical platforms, among which electromagnetism and plasmonics,[21,22] acoustics,[23] and via elastic structures.[24–26] The key idea is to take advantage of the resonator-structure interactions to gradually nullify the wave velocity in space. This modulation strategy induces energy trapping in a frequency-dependent position along the grading, which is known to be convenient for energy harvesting purposes as compared to perfectly periodic configurations or to other forms of energy localization.[27] As a further step in this direction, this paper investigates the vibration attenuation and energy harvesting capabilities of a hybrid electromechanical graded metastructure. The implementation consists of a beam equipped with both mechanical (with bonded non-resonating piezo-layers) and electromechanical resonators, initially tuned at the same frequency to create a single gap, in analogy to the behavior reported in Ref. 28. We investigate the role of different grading laws on the attenuation characteristics of the underlying medium. In addition, we consider that each resonator can be used to harvest energy at its corresponding natural frequency. We analyze the energy harvesting capabilities of such a system in comparison to non-graded configurations and to the graded electromechanical metastructure presented in Ref. 24.

II. ANALYTICAL FRAMEWORK

We consider the metastructure illustrated in Fig. 1, in the attempt to combine the two bodies of work[24,28] and to show the energy harvesting capabilities of such a system. The structure is made of a cantilever beam with a number $S = 25$ of periodically placed pairs of piezoelectric patches (parallel-wire operation) equipped with RL circuits, which constitute a set of electromechanical resonators when connected to the piezo-elements. Additionally, the electromechanical beam, which at this step is analogous to the one studied in Ref. 24, is further augmented by a pattern of mechanical resonators according with the schematic shown in the figure. In contrast to Ref. 28, the mechanical resonators employed herein are cantilever bimorph with series-connected non-resonating resistive loads. To ease readability, the relevant parameters are listed in the nomenclature and hereafter employed to define the elasto-dynamic equations of the system:

$$EI\frac{\partial^4 w}{\partial x^4} + m\frac{\partial^2 w}{\partial t^2} - \theta^c \sum_{j=1}^{S} v_j^c \left(\frac{\partial \delta(x - x_j^L)}{\partial x} - \frac{\partial \delta(x - x_j^R)}{\partial x} \right) + \sum_{j=1}^{S} (k_j u_j + c_j \dot{u}_j)\delta(x - x_j) = -m\ddot{w}_b, \tag{1a}$$

$$C_p^c \dot{v}_j^c + Y_j^c v_j^c + \theta^c \int_{x_j^L}^{x_j^R} \frac{\partial^3 w}{\partial x^2 \partial t}\, dx = 0, \tag{1b}$$

$$m_j\left(\ddot{u}_i + \ddot{w}(x_j) + \ddot{w}_b\right) + c_j\dot{u}_j + k_j u_j - \theta_j^r v_j^r = 0, \tag{1c}$$

$$C_p^r \dot{v}_i^r + Y_j^r v_j^r + \theta_j^r \dot{u}_i = 0, \tag{1d}$$

where $w(x, t)$ is the transverse vibration relative to the base motion $w_b(x, t)$. u_j is the tip displacement of the jth resonator and $v_j^{c,r}(t)$ is the voltage across the jth patch bonded at a coordinate x_j, where the superscript c, r denotes the hosting medium for the patch, which can be either the cantilever (c) or the resonators (r). Here, the physical and elastic properties of the composite structure are

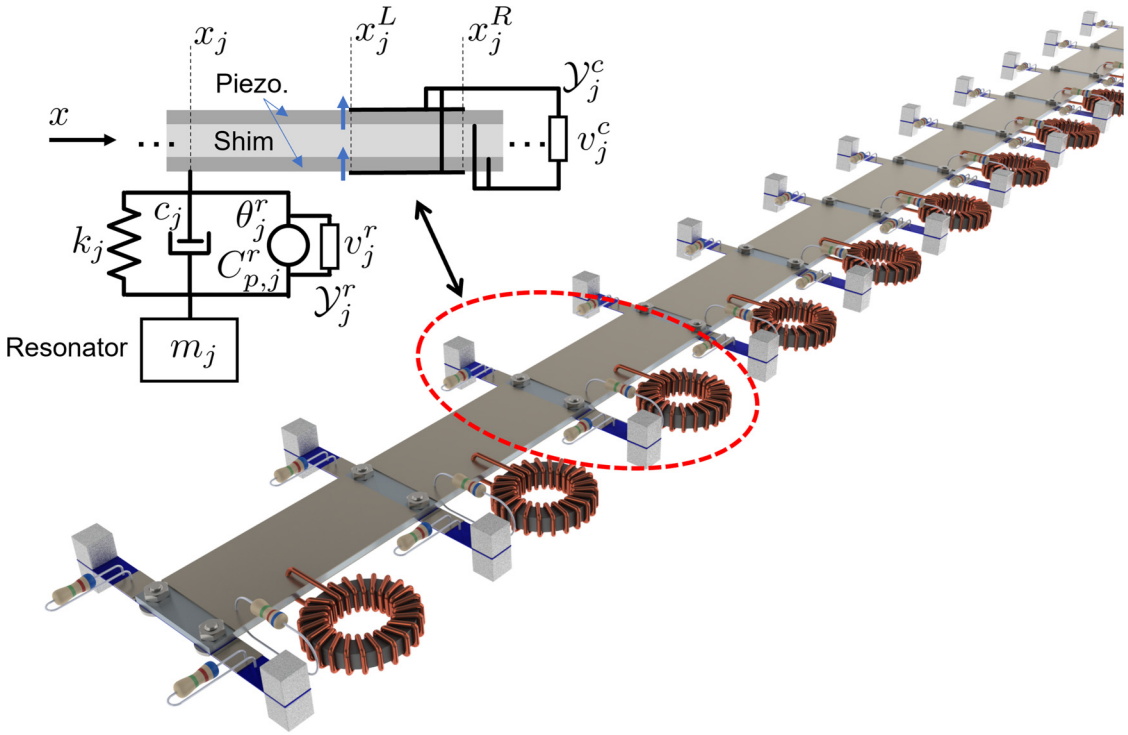

FIG. 1. Schematic of the hybrid electromechanical graded structure. The inset shows a side view of a single pair of mechanical and electromechanical resonators.

described in terms of equivalent properties,

$$EI = \frac{2b^c}{3}\left(c_s h_s^c + c_{11}^E\left[\left(h_p^c + \frac{h_s^c}{2}\right)^3 - \frac{(h_s^c)^3}{8}\right]\right), \tag{2a}$$

$$m = b^c\left(\rho_s h_s^c + 2\rho_p h_p^c\right), \tag{2b}$$

$$\theta^c = \frac{\bar{e}_{31} b_s^c}{2h_p}\left[\left(h_p^c + \frac{h_s^c}{2}\right)^2 - \frac{(h_s^c)^2}{4}\right], \tag{2c}$$

$$C_p^c = \bar{\varepsilon}_{33}^S b^c \frac{\left(x_j^R - x_j^L\right)}{2h_p^c}, \quad C_p^r = \bar{\varepsilon}_{33}^S b^r \frac{L^r}{2h_p^r}. \tag{2d}$$

Approximate solutions of the elastodynamic equation (1) are sought in terms of assumed mode expansion $w(x,t) = \sum_{q=1}^{N} \phi_q(x)\eta_q(t)$, where $\phi(x)$ and $\eta(t)$ are the plain beam mass-normalized mode shapes and corresponding generalized coordinates with unknown amplitudes, respectively. Through Eq. (1) and due to orthogonality conditions,[19] we get to a set of ordinary differential equations of dimension $4N$ with $N = 200$ number of modes employed in the expansion of $w(x,t)$,

$$\ddot{\eta}_k + 2\zeta_k\omega_k\dot{\eta}_k + \omega_k^2\eta_k - \theta^c\sum_{j=1}^{S} v_j^c\Delta\phi_{kj}' + \sum_{j=1}^{S}\left(k_j u_j + c_j\dot{u}_j\right)\phi_k(x_j) = -m\ddot{w}_b\int_0^L \phi_k(x)\,dx, \tag{3a}$$

$$C_p^c\dot{v}_j^c + Y_j^c v_j^c + \theta^c\sum_{q=1}^{N}\Delta\phi_{qj}'\dot{\eta}_q = 0, \tag{3b}$$

$$\ddot{u}_j + 2\zeta_j\omega_j^r\dot{u}_j + \omega_j^{r2}u_j - \theta_j^r v_j^r = -\ddot{w}_b - \sum_{j=1}^{S}\phi_q(x_j)\ddot{\eta}_q, \tag{3c}$$

$$C_p^r\dot{v}_j^r + Y_j^r v_j^r + \theta_j^r\dot{u}_j = 0, \tag{3d}$$

where ω_k is the kth characteristic frequency of the plain beam, $\zeta_k = 0.001$ is the corresponding dimensionless damping ratio, and ω_j^r and $\zeta_j = 0.001$ are the jth mechanical resonator resonant frequency and damping ratio, respectively. We also define the term $\Delta\phi_{kj}' = \frac{d\phi_k}{dx}\big|_{x_j^L}^{x_j^R}$, which modulates the piezoelectric coupling of the corresponding generalized coordinate and is dependent on the

spacing between resonators. We now apply Laplace transform to the dynamic quantities, and after a few mathematical manipulations to get to

$$\left(s^2+2\zeta_k\omega_k s+\omega_k^2\right)H_k(s)+s(\theta^c)^2\sum_{q=1}^{N}\sum_{j=1}^{S}\frac{\Delta\phi'_{kj}\Delta\phi'_{qj}}{C_p^c\left(s+h_j^c(s)\right)}H_q(s)$$
$$+s^2\sum_{q=1}^{N}\sum_{j=1}^{S}\frac{\mu\Delta x\left(\omega_j^{r2}+2\zeta_j\omega_j^r s\right)m\phi_q(x_j)\phi_k(x_j)}{s^2+2\zeta_j\omega_j^r s+\omega_j^{r2}\left(1+\frac{s\gamma}{s+h_j^r(s)}\right)}H_q(s)=Q_k(s), \tag{4a}$$

$$C_p^c\left(s+h_j^c(s)\right)V_j^c(s)+s\theta^c\sum_{j=1}^{S}\Delta\phi'_{qj}H_q(s)=0, \tag{4b}$$

$$\left(s^2+2\zeta_j\omega_j^r s+\omega_j^{r2}\left(1+\frac{s\gamma}{s+h_j^r(s)}\right)\right)U_j(s)=Q_q(s), \tag{4c}$$

$$C_p^r\left(s+h_j^r(s)\right)V_j^r(s)+s\theta_j^r U_j(s)=0, \tag{4d}$$

where $H_k(s)$, $U_j(s)$, $V_j^c(s)$, and $V_j^r(s)$ are the Laplace transformed forms of $\eta_k(t)$, $u_j(t)$, $v_j^c(t)$, and $v_j^r(t)$, which are evaluated inverting the system of Eq. (4). The forcing terms $Q_k(s)$ and $Q_q(s)$ are

$$Q_k(s)=-s^2mW_b(s)\left(\int_0^L\phi_k(x)\,dx\right.$$
$$\left.+\sum_{j=1}^{S}\frac{\mu\Delta x\left(\omega_j^{r2}+2\zeta_j\omega_j^r s\right)\phi_k(x_j)}{s^2+2\zeta_j\omega_j^r s+\omega_j^{r2}\left(1+\frac{s\gamma}{s+h_j^r(s)}\right)}\right), \tag{5}$$
$$Q_q(s)=-s^2\left(W_b(s)+\sum_{q=1}^{N}\phi_q(x_j)H_q(s)\right).$$

Here, $W_b(s)$ is the base motion in the Laplace domain. Δx is the spacing between mechanical resonators, $\mu=1$ and $\gamma=0.1$ are dimensionless parameters which, along with ω_j^r and ω_j, set the limits of locally resonant frequency gaps for uniform configurations,[28]

$$\mu=\frac{\sum_{j=1}^{S}m_j}{mL},\quad \gamma=\frac{\left(\theta_j^r\right)^2}{k_jC_p^r}, \tag{6}$$

where h_j^c and h_i^r are the normalized admittances across the jth electrode pair for the patches on the cantilever beam and the mechanical resonators,

$$h_j^c(s)=\frac{(\omega_j^c)^2}{s}+\frac{1}{\tau_j^c},\quad h_j^r(s)=\frac{1}{\tau_j^r}, \tag{7}$$

where ω_j^c is the resonance frequency of the jth shunt circuit and $\tau_j^c=C_p^cR_j^c$ and $\tau_j^r=C_p^rR_j^r$ are the time constants. Following Ref. 24, we explore different configurations by letting ω_k vary along the beam main dimension according to different laws,

$$\omega_k^{r,c}=\omega_t+\Delta\omega_{r,c}-2\Delta\omega_{r,c}\left(\frac{k-1}{S-1}\right)^p,\quad k=1,\ \ldots,S, \tag{8}$$

where $\omega_t=35\,\omega/\omega_1$ serves as the central frequency of the grading and non-graded configurations can be restored by letting $\Delta\omega\to0$. In the case at hand, we set $\tau^r\omega_t=500$ and $\tau^c\omega_t=500$. $2\Delta\omega$ and p are the grading range and order of the resonator pattern, while the numerical values of the geometry and the material properties are listed in Table I. We remark that, in the case of uniform configurations, each resonator can be linked to a theoretical gap limit (see Ref. 28). In contrast, graded metastructures lack translation symmetry and the definition of bandgaps is elusive. However, when the modulation of $\omega_k^{r,c}$ is sufficiently slow (i.e., in absence of abrupt changes), the dynamic characteristics of the beam at a given coordinate $x=k\Delta x$ can be qualitatively associated to that of the medium equipped with the kth resonators.[25] Hence, it is expected that spatially dependent attenuation regions are generated through different distributions of $\omega_k^{r,c}$ and that such regions are consistent with the gap limits evaluated through the theoretical framework presented in Ref. 28. This aspect is further discussed in the following and supported by numerical results.

TABLE I. Geometrical and material properties of the hybrid metastructure.

Parameter	Value	Unit
h_s^c	1	mm
b^c	10	mm
$\bar{c}_{11}^E$	61	GPa
ρ_p	7750	kg m^{-3}
$\bar{\epsilon}_{33}^S$	13.3	nF m^{-1}
b^r	2	mm
ρ_s	2700	kg m^{-3}
c_s	69	GPa
$h_p^{c,r}$	0.3	mm
$\bar{e}_{31}$	−12.3	C m^{-2}
L^r	20	mm
L	0.1	m

III. NUMERICAL RESULTS AND DISCUSSION

The analysis of the system is accomplished through a number of combinations for p, i.e., fractional order $p=1/2$, linear $p=1$, and quadratic $p=2$. Also, different frequency ranges are spanned for both mechanical and electromechanical resonators through different combinations of $\Delta\omega_{c,r}$. For each of the aforementioned grading orders, four distinct configurations are used: $\Delta\omega_c=\Delta\omega_r=-3$ and $\Delta\omega_c=\Delta\omega_r=3$, which correspond to electrical and mechanical resonances spanning the same frequency range toward positive and negative values. As such, the mechanical and electromechanical attenuation regions are expected to merge, but not to overlap.[28] $\Delta\omega_c=-\Delta\omega_r=-3$, and $\Delta\omega_c=-\Delta\omega_r=3$, are instead tailored to

move the mechanical and electromechanical resonances in an opposite fashion, whereby the mechanical attenuation region that is initially tuned at higher (lower) frequencies, and the electromechanical attenuation region initially tuned at lower (higher) frequency values are expected to merge upon varying ω_k in space. Note that, on one hand, $\Delta\omega_{c,r}$ is chosen sufficiently slow to avoid spatial discontinuities along the beam. On the other hand, too small $\Delta\omega_{c,r}$ values would have led to minor differences as compared to uniform configurations.

We start the discussion with the analysis of the tip response of the cantilever, which is displayed in Fig. 2. It is interesting to notice that all the probed configurations, represented by colored lines, feature good attenuation capabilities for a wide frequency range. Moreover, similarly to the uniform configuration (black dashed line), i.e., when all the resonators are tuned at the same frequency, the transmissibility value $|w_{abs}(L)/w_b|$ drops of approximately 2 orders of magnitude. This suggests that graded structures can be suitably employed for vibration control purposes and that the grading does not reduce the filtering capabilities of the periodic system. Another important outcome is the formation of a narrow frequency range populated by a number of resonances. Such a range is known to emerge in uniform configurations due to the finite number of resonators. A similar (but conceptually different) behavior is observed for structures with opposite grading law which, instead, is caused by concurrent negative stiffness and negative mass effects.[28] Finally, we observe that, in general, a number of sharp resonances can populate the response, corresponding to localized modes whose properties are liked to the characteristics of the grading profile. To shed light on this matter, the frequency response of the entire cantilever is evaluated within $x \in [0, L]$ and displayed in Figs. 3–5 in the neighborhood of $\omega_t = 35\,\omega/\omega_1$, with superimposed grading laws for the electromechanical and

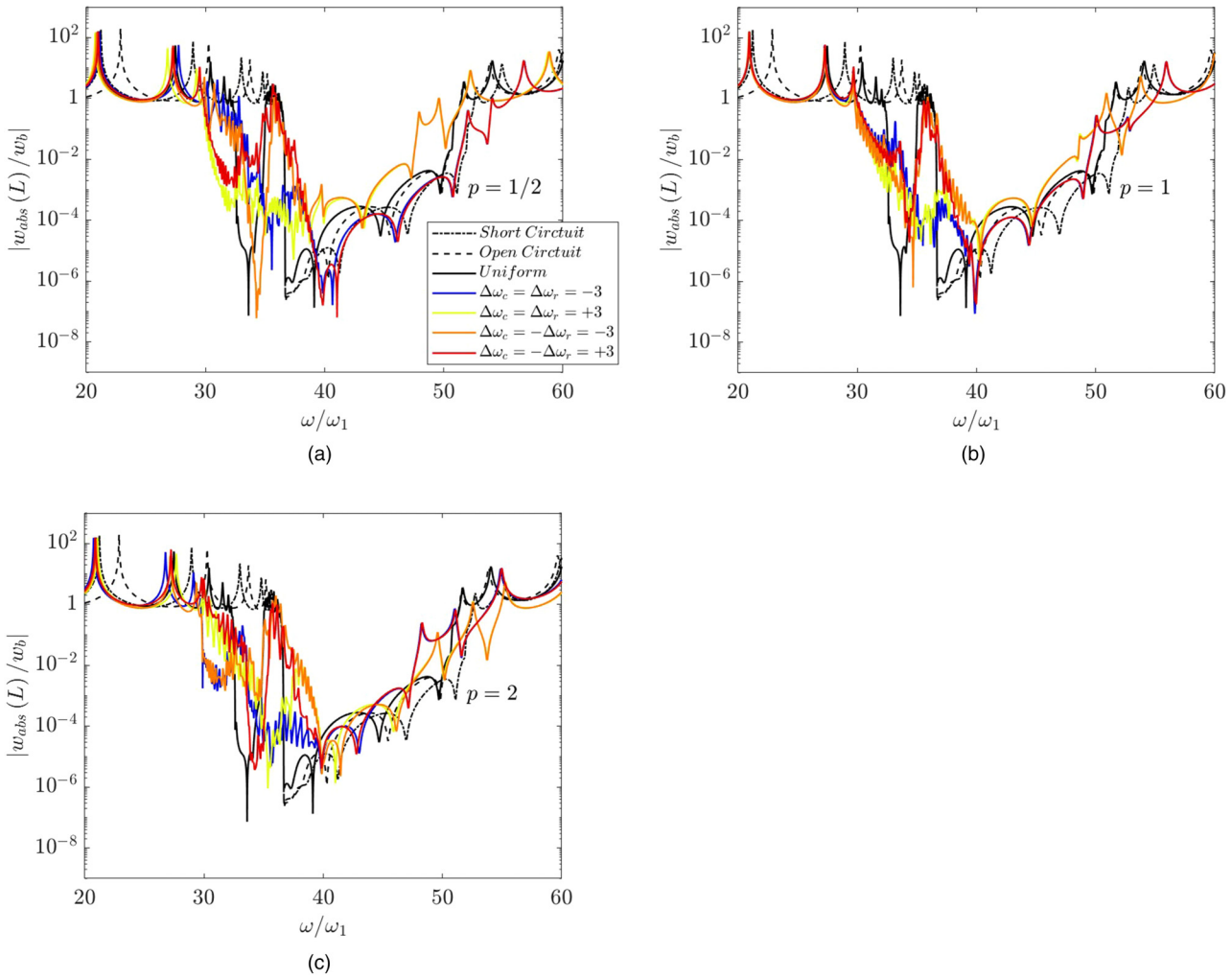

FIG. 2. Beam tip transmissibility vs normalized excitation frequencies for different grading ranges and grading patterns with (a) $p = 1/2$, (b) $p = 1$, and (c) $p = 2$.

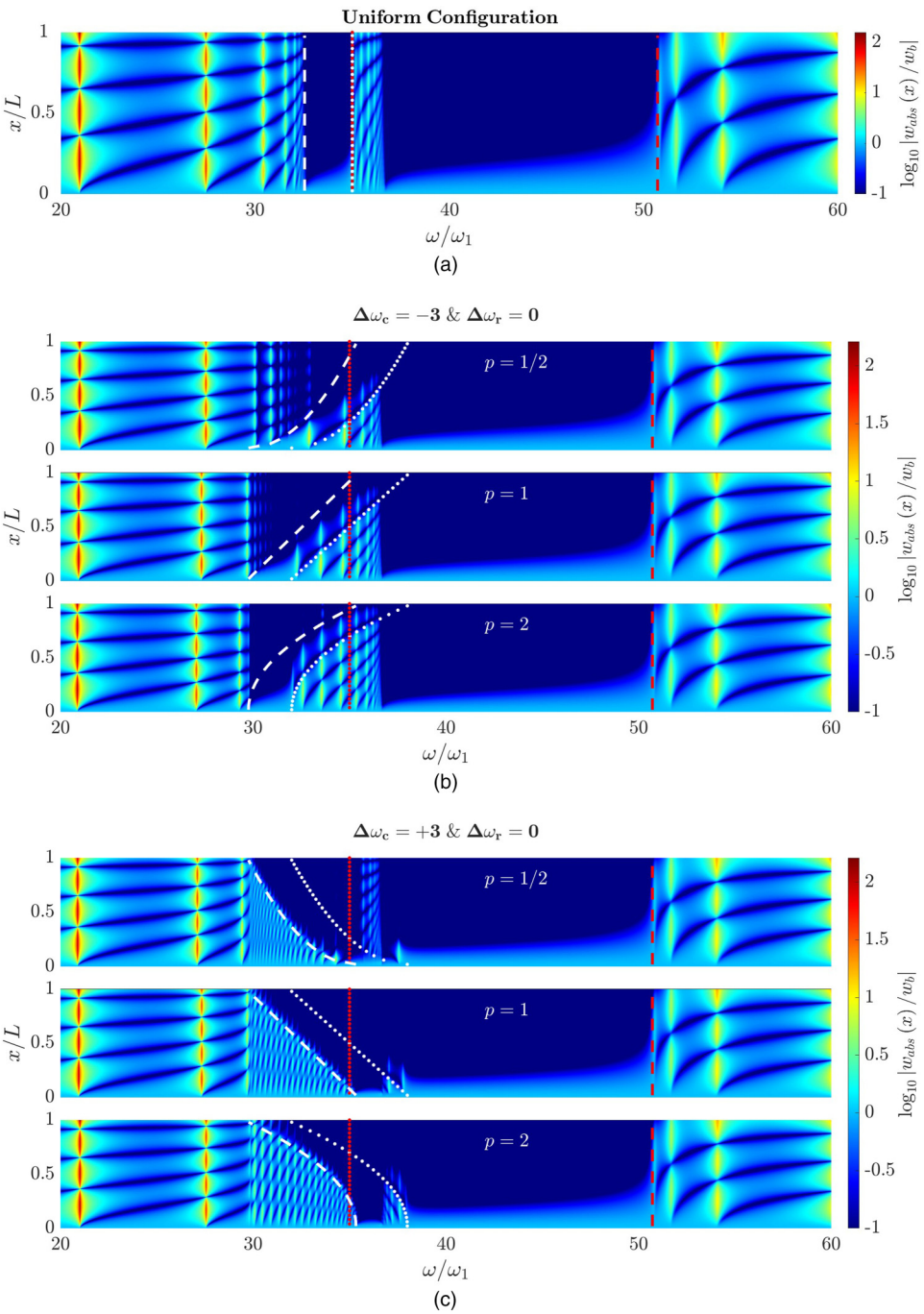

FIG. 3. Displacement response upon varying normalized excitation frequencies and normalized beam length for (a) the uniform metastructure and [(b) and (c)] a hybrid metastructure with graded electromechanical resonators and uniform mechanical resonators for $\Delta\omega_c = \pm 3$ and different grading patterns $p = 1/2$, $p = 1$, and $p = 2$. White and red dots represent the resonant frequency of the electromechanical and mechanical resonators, respectively. Dashed lines represent the bandgap limits evaluated through the theoretical formulation presented in Ref. 28.

mechanical resonators (white and red dots) and the corresponding theoretical bandgap limits (white and red dashed lines). We remark that such limits provide an indication about the spatial separation between localized modes and attenuation regions generated through the grading but, due to the interplay between electromechanical and mechanical resonators, additional modes can be generated.[28] Some considerations follow. (i) If the grading law for the mechanical and electromechanical resonators is the same, a single and complete attenuation region can form (Figs. 3 and 4). Under this condition, there are a number of modes that populate the neighborhood of the tuning frequency ω_t and, interestingly, such modes are characterized by low amplitude and become less

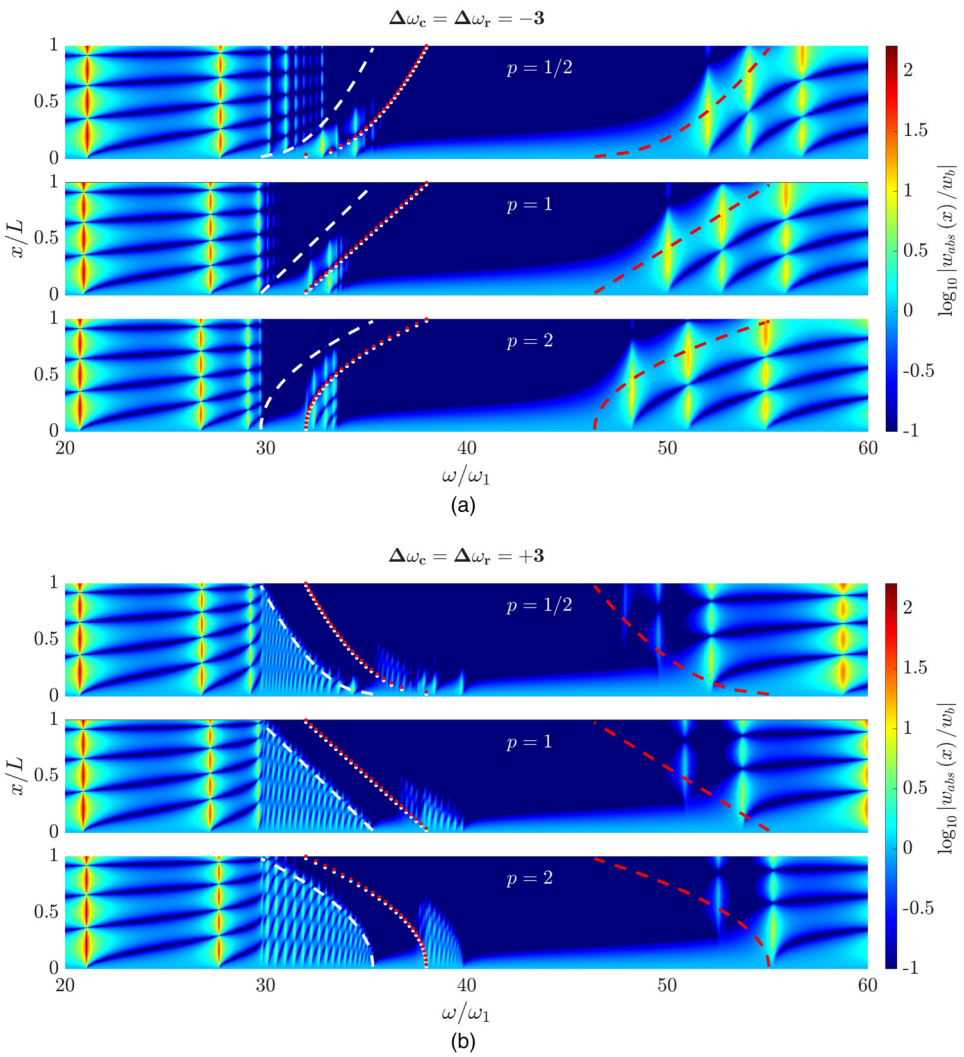

FIG. 4. Displacement response upon varying normalized excitation frequencies and normalized beam length for [(a) and (b)] $\Delta\omega_c = \Delta\omega_r = \pm 3$ and different grading patterns $p = 1/2$, $p = 1$, and $p = 2$. White and red dots represent the resonant frequency of the electromechanical and mechanical resonators, respectively. Dashed lines represent the bandgap limits.

relevant for points located toward the tip of the cantilever. We observe that such modes are instead very relevant in the case of uniform configurations [Fig. 3(a)] and that their amplitude decreases as the electromechanical [Figs. 3(b) and 3(c)] or both electromechanical and mechanical gradings (Fig. 4) are activated. (ii) There is the formation of localized modes due to the gradual variation of the characteristic frequency ω_k in space, especially for frequencies in the neighborhood of the theoretical bandgap limits (i.e., the white and red curves), which are evaluated under the assumption of quasi-static evolution of the grading. As such, the localization properties of such modes follow the shape of the graded profile and, for a fixed frequency, we observe a variable wavelength in space, which is particularly evident in Figs. 4(b) and 5(b) and is the blueprint of the rainbow effect. The transition between uniform distribution [Fig. 3(a)] and graded configurations (Figs. 4 and 5) confirms that the generation of localized modes is dictated by the gap limits and we also remark that such modes can be conveniently employed for energy harvesting purposes and further discussed later in the paper. (iii) There are regions in which the localization properties do not follow the modulation profile, which are instead dictated by the overlapping between distinct bandgaps and, therefore, present only within shared regions between the expected electromechanical and mechanical gap limits, e.g., around 36 ω/ω_1 in Fig. 5(b). These latter are visible also in the red and orange transmission curves in Fig. 2, i.e., when the grading laws have opposite directions. As a final comment on this part, we remark that the emergence of localized modes is justified by two distinct phenomena associated with the grading. The first is associated with the rainbow effect which yields localized modes in the vicinity of the expected bandgap limits. The second is instead associated with the merging and overlapping of the expected frequency gaps. In both cases, the spatial separation between attenuation and localization regions is consistent with the gap limits evaluated through the theoretical framework presented in Ref. 28.

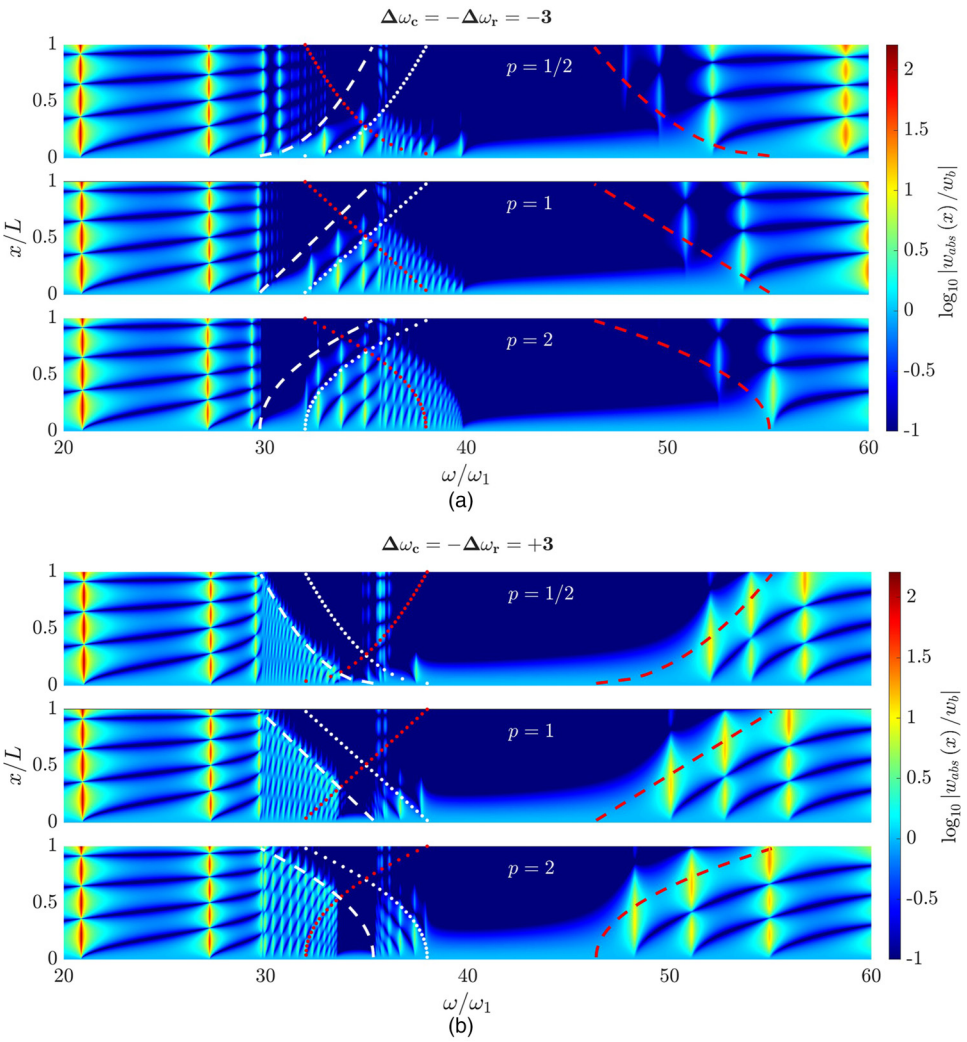

FIG. 5. Displacement response upon varying normalized excitation frequencies and normalized beam length for [(a) and (b)] $\Delta\omega_c = -\Delta\omega_r = \pm 3$ and different grading patterns $p = 1/2$, $p = 1$, and $p = 2$.

We now discuss the energy harvesting capabilities of the system and we remark that the performance is to be compared to the ungraded system and to the ones presented in Ref. 24. First and foremost, we note that the amount of power does depend on the resistive loads $R_j^{c,r}$ and, to provide a fair comparison between different configurations, $\tau^{r,c}\omega_t = 500$ is arbitrarily set constant for all the circuits. Now, to clarify the role of the grading on the system performance, the overall output power per base acceleration fed in all resonators is illustrated in Figs. 6 and 7, along with the average power (Figs. 8 and 9) integrated over the region of interest $\omega/\omega_1 \in [30, 35]$ and $\omega/\omega_1 \in [30, 40]$. Such regions are chosen to include the resonating frequency of the resonators along the grading, which are responsible for most of the harvested power. The former (green box) is the same range studied in Ref. 24, while the latter (blue box and green box) is the range spanned by the resonating elements of the hybrid configuration. Different configurations are displayed in Figs. 6 and 7, in order to qualify the transition between a purely electromechanical graded metastructure, a hybrid configuration with graded electromechanical resonators, and a graded metastructure with both electromechanical and mechanical graded array of resonators. Interestingly, we observe the emergence of several resonance peaks when $\Delta\omega \neq 0$ and when at least one grading is activated, corresponding to the localized modes discussed above. In the context of energy harvesting, high amplitude and great density of modes is favorable and reflects into improved power output as compared to ungraded configurations, especially for broad excitation spectra. This is visible on the histograms displayed alongside the response in Figs. 8 and 9, which represent the average power within the green and blue-highlighted regions for the three different case-studies illustrated in Figs. 6 and 7 (i.e., graded electromechanical resonators, graded electromechanical resonators with ungraded mechanical resonators, and graded electromechanical with mechanical resonators) and for grading order $p = 1/3$, $p = 1/2$, $p = 1$, $p = 2$, and $p = 3$. Specifically, the first bar is related to the results shown in Ref. 24 and, therefore, without the mechanical resonators. The second and the third are relative to the hybrid metastructure with uniform and

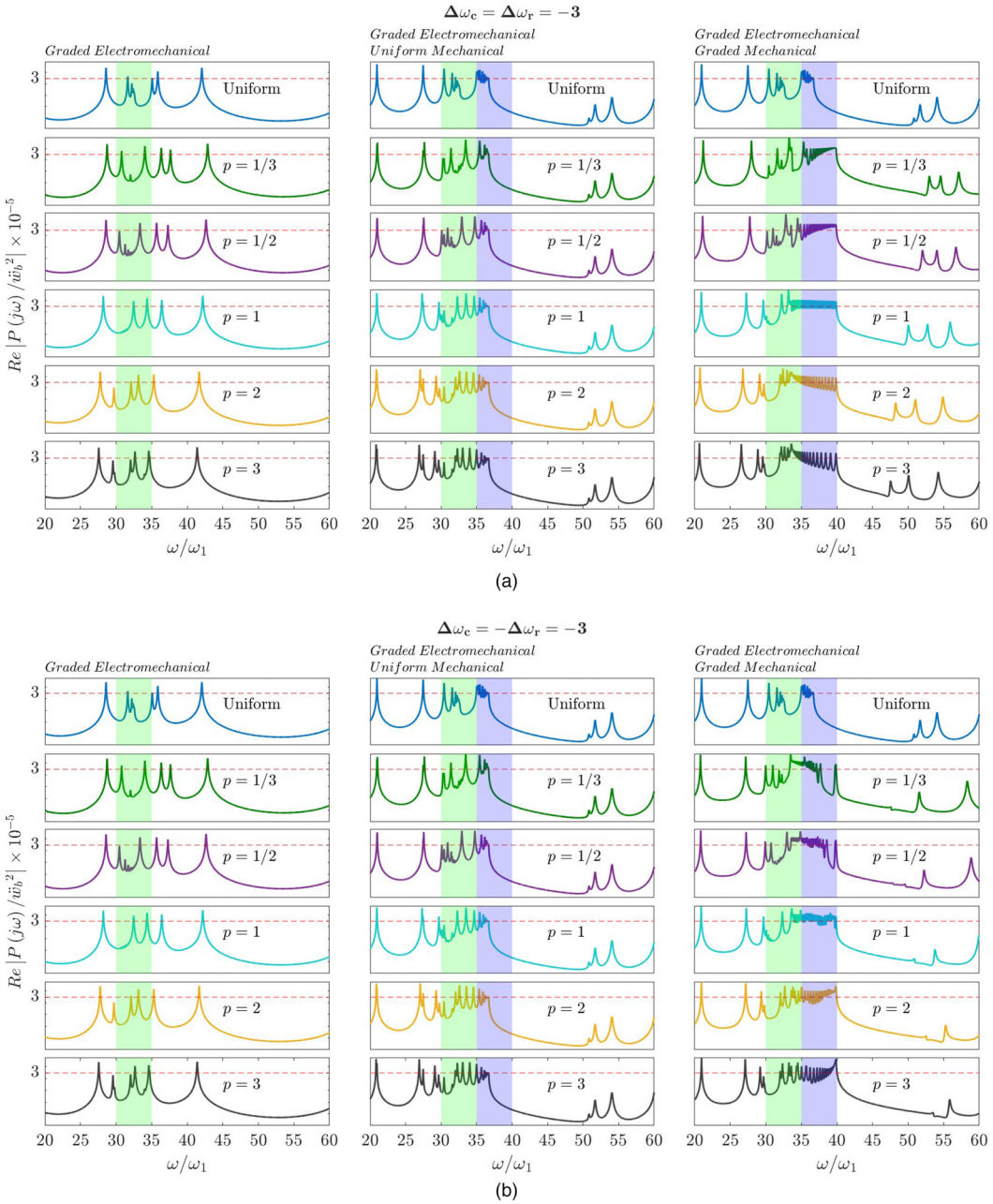

FIG. 6. Frequency response (real part) relative to the power fed into all resonators in the case of (a) $\Delta\omega_c = \Delta\omega_r = -3$ and (b) $\Delta\omega_c = -\Delta\omega_r = -3$ with grading patterns $p = 1/3$, $p = 1/2$, $p = 1$, $p = 2$, and $p = 3$. Real part of the power output response harvested from the array of electromechanical resonators for a structure equipped with solely electromechanical resonators (left). Real part of the power output response harvested from both mechanical and electromechanical attachments when the grading is applied only to the electromechanical resonators (center). Real power output harvested from the hybrid metastructure equipped with both mechanical and electromechanical graded distributions of resonators (right).

graded distribution of the mechanical resonators, respectively, integrated over the green region to provide a fair comparison. The fourth and fifth bars represent the average power relative to the hybrid metastructure with uniform and graded distribution of the mechanical resonators but integrated within both blue and green regions. We first observe that all the analyzed grading patterns feature improved power output as compared to the uniform system, which suggests that graded configurations are well suited not only for

vibration control purposes but also for energy harvesting problems. A careful analysis of the power diagrams reveals that a great amount of power is fed into the mechanical resonators, which are responsible for a notable increase of power output as compared to the configuration with purely electromechanical resonators,[24] and that the activation of their grading reflects into a further increase of the output power as compared to mixed graded-uniform distributions. In addition, we notice a relevant improvement of the power output when the bandwidth is extended from $\omega/\omega_1 \in [30, 35]$ to $\omega/\omega_1 \in [30, 40]$, again motivated by the additional energy fed into

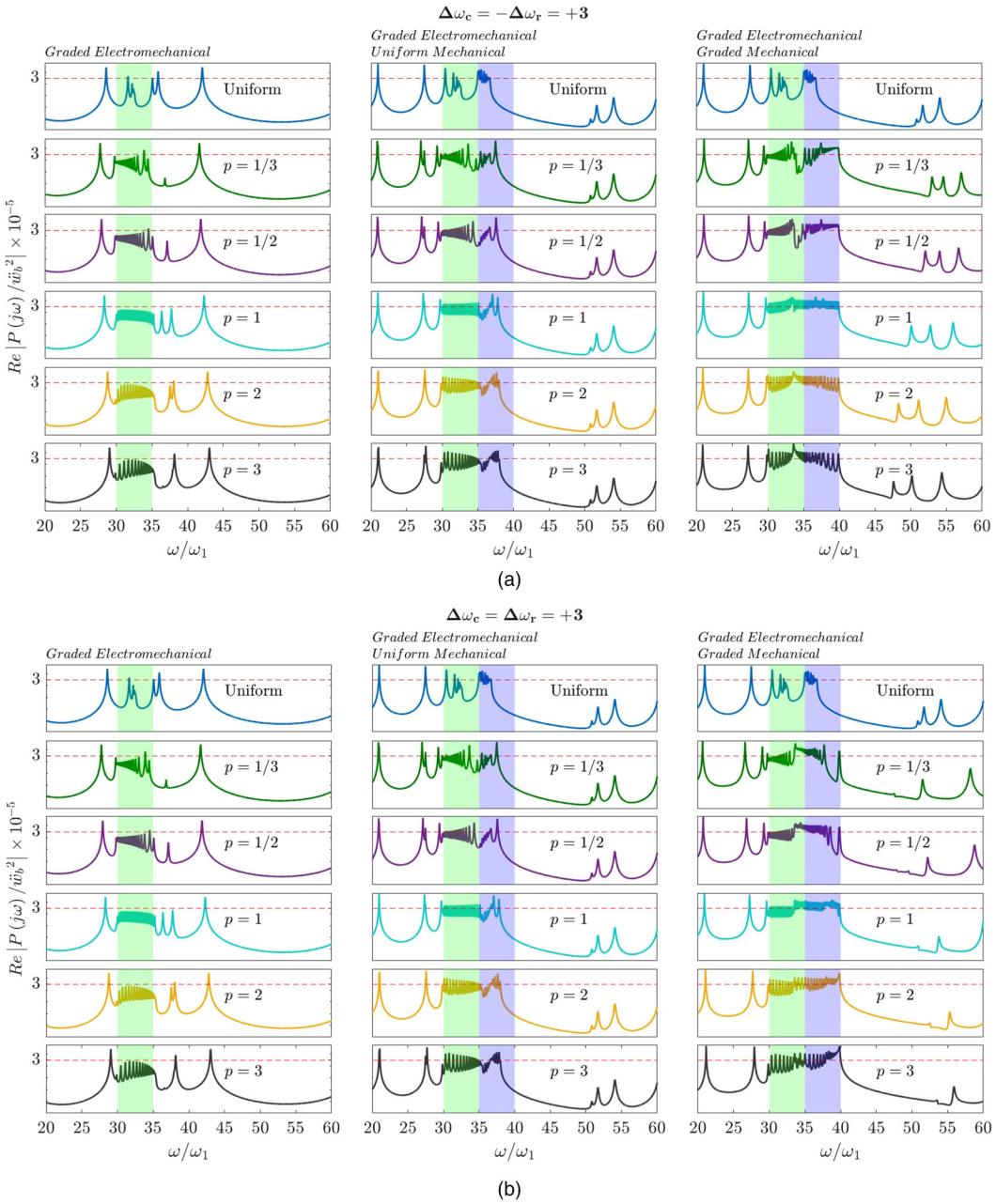

FIG. 7. Frequency response (real part) relative to the power fed into all resonators in the case of (a) $\Delta\omega_c = -\Delta\omega_r = +3$ and (b) $\Delta\omega_c = \Delta\omega_r = +3$ with grading patterns $p = 1/3$, $p = 1/2$, $p = 1$, $p = 2$, and $p = 3$.

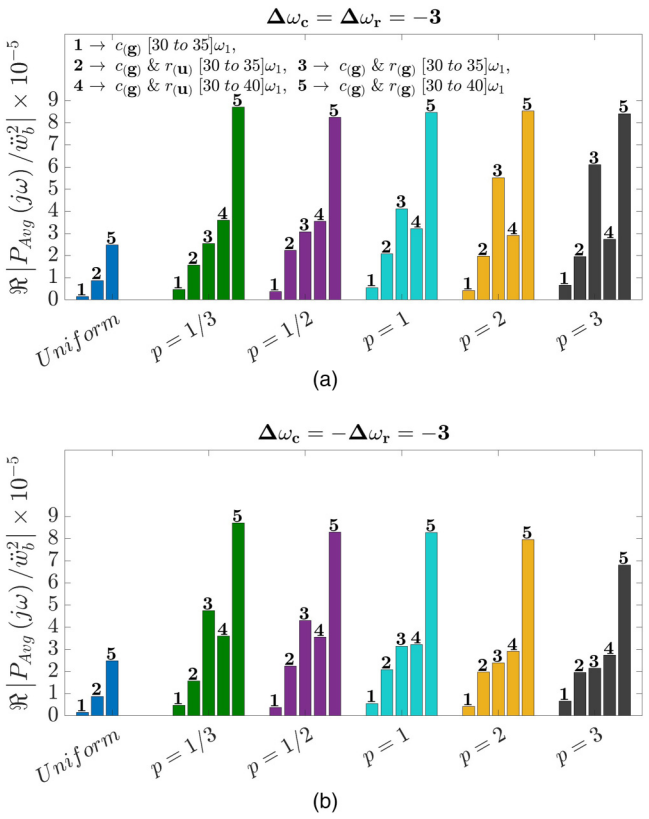

FIG. 8. Average power integrated over the shaded regions displayed in Fig. 6 for (a) $\Delta\omega_c = \Delta\omega_r = -3$ and (b) $\Delta\omega_c = -\Delta\omega_r = -3$ with grading patterns $p = 1/3$, $p = 1/2$, $p = 1$, $p = 2$, and $p = 3$. The first bar illustrates the average power within the green region when the mechanical resonators are not present, which corresponds to Ref. 24. The second bar is the averaged power of the hybrid metastructure integrated over the green range when the grading is activated only for the electrical resonators. The third bar is relative to the hybrid configuration with both graded and ungraded distributions averaged over the green range. The fourth bar represents the average power within the green and blue regions for the hybrid metastructure when the electromechanical resonators are graded and the mechanical resonators are uniform. The fifth bar is relative to the average power for the hybrid metastructure with graded electromechanical and mechanical resonators over the green and blue regions.

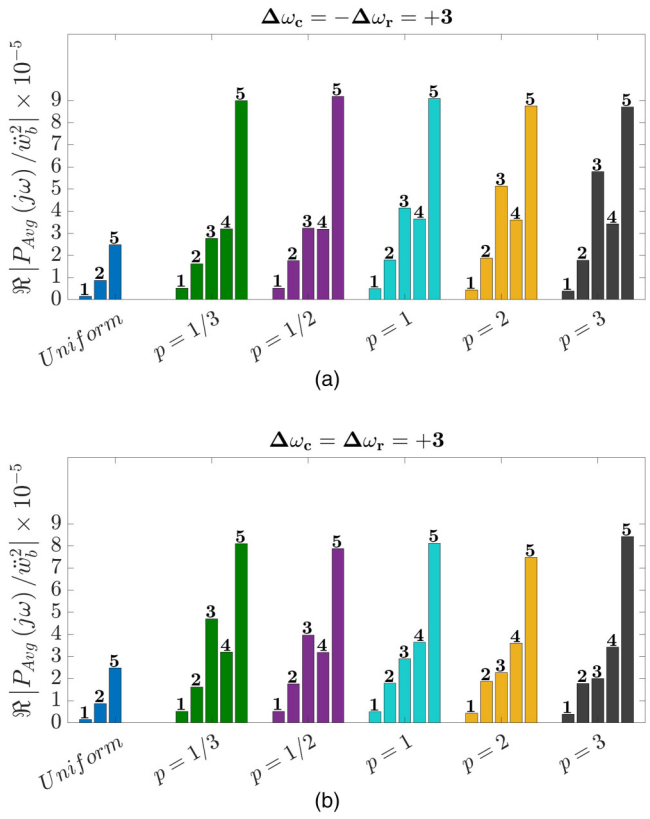

FIG. 9. Average power integrated over the shaded regions displayed in Fig. 7 for (a) $\Delta\omega_c = -\Delta\omega_r = +3$ and (b) $\Delta\omega_c = \Delta\omega_r = +3$ grading patterns with $p = 1/3$, $p = 1/2$, $p = 1$, $p = 2$, and $p = 3$.

the mechanical resonators. The comparison between different grading orders p instead suggests that all the configurations employed in the paper are capable of providing similar improvements in terms of power output. We finally remark, however, that different grading profiles determine different attenuation and localization characteristics in space.

To conclude the discussion and to better qualify the role of each resonators, we show how the power frequency response, the average power, and the percentage of harvested power integrated within the green and blue boxes modify for consecutive resonators in space. Note that similar considerations apply for all the grading directions employed in the paper and, therefore, for simplicity, we only show the power response relative to $\Delta\omega_c = \Delta\omega_r = -3$ and we summarize all results in terms of average and percentage power plots. We start considering the power output results for a beam without mechanical resonators,[24] which are illustrated in Fig. 10(a) upon varying frequency and resonator index (hence position). Here, in contrast to uniform configurations, the peak power is not limited in the neighborhood of a single frequency but follows the grading order, which reflects into improved energy harvesting capabilities. The response is later numerically integrated within the green-highlighted region (i.e., $\omega/\omega_1 \in [30, 35]$) and displayed in Figs. 10(b) and 10(c) in terms of average power output and percentage power output. It can be observed that, for uniform configurations, the amount of average power is, in general, lower as compared to graded systems and, interestingly, the amplitude suddenly drops after the first resonators, which is attributed to the locally resonant metamaterial behavior and bandgap formation mechanisms. In other words, graded systems offer higher output power amplitude locally, and more resonators are involved in the structural motion, which justifies the improved average power output when a certain law of variation is considered. A stronger but analogous effect is observable if also the mechanical resonators are connected to the host beam. Under these conditions, the power

responses measured for consecutive electro-mechanical and mechanical resonators are illustrated in Fig. 11 along with the average and percentage power in Fig. 12, separating the contributions from the electromechanical [Figs. 12(a) and 12(b)] and mechanical resonators [Figs. 12(c) and 12(d)]. It can be noticed that the spectral content observed in the power response (Fig. 11) is consistent with the localization properties displayed in Fig. 4(a) and, also, the peak power follows the grading order in the frequency–space diagrams. Also here, due to the bandgap formation mechanisms, there is a sudden drop in the power after a few unit cells for uniform configurations [see Figs. 12(c) and 12(d)]. Conversely, graded configurations display higher values in amplitude and, consistently with the above discussion, are justified by the formation of local resonances within the relevant frequency range. The interplay among these effects reflects into greater average power and percentage power output gathered over a certain bandwidth from the electromechanical and mechanical resonators. This effect is particularly evident from the amount of power fed into the mechanical resonators [Figs. 12(c) and 12(d)], which is almost equally distributed along space and further demonstrates the enhanced bandwidth of the graded metastructure. In summary, a flat power distribution is favored by the design of graded profiles, which is justified by the spatial localization of standing modes occurring at different frequencies. This feature guarantees improved average power output for all the grading orders p and for the distinct combination of $\Delta\omega_{c,r}$ analyzed in the paper. Practically, graded configurations favor the activation of the array of resonators over a broader range of frequencies, which is here captured by the total power frequency response fed into all resonators (Figs. 6 and 7), from its frequency average (Figs. 8 and 9), and by the power response in space (real power, average power, and percentage power in Figs. 10–12).

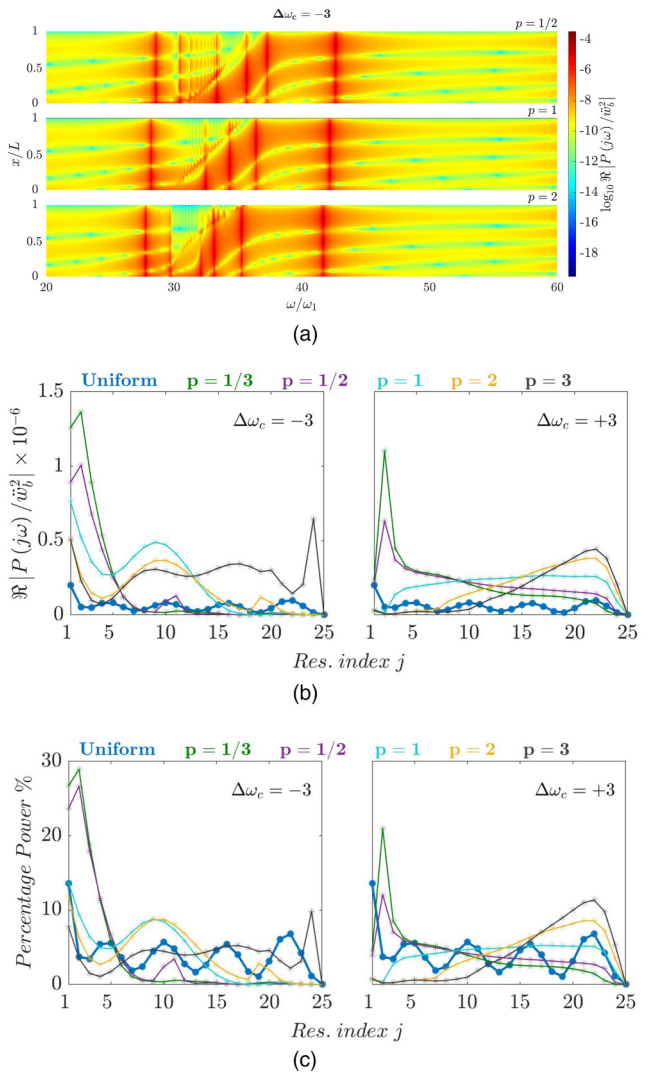

FIG. 10. (a) Real part of the power frequency response upon varying the resonators in space for a structure equipped with only electromechanical resonators and with grading range $\Delta\omega_c = -3$. (b) Average and (c) percentage power (upon varying the attachment index j) integrated within $\omega/\omega_1 \in [30-35]$ for the grading ranges $\Delta\omega_c = \pm 3$.

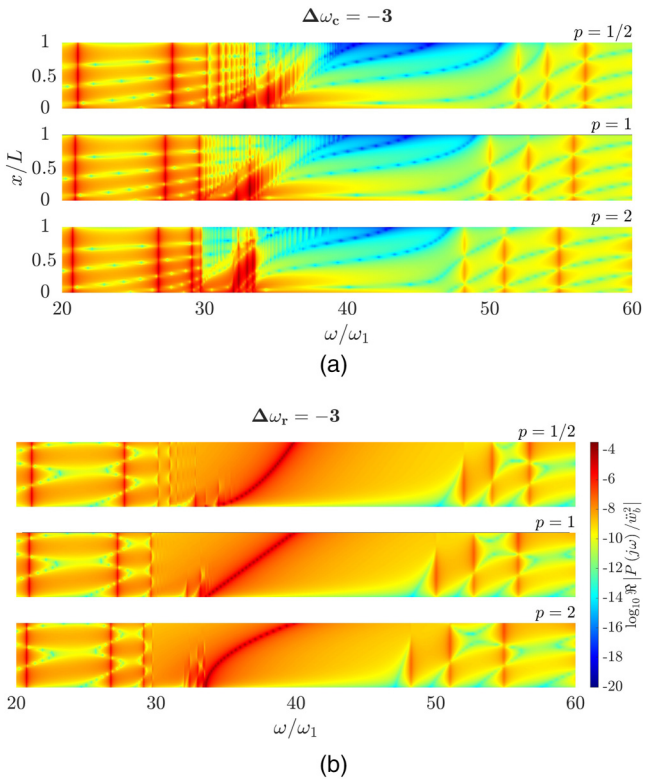

FIG. 11. Real part of the power frequency response measured on consecutive resonators in space for a structure equipped with both electromechanical and mechanical resonators. (a) The power fed into the electromechanical resonators. (b) The power fed into the mechanical resonators.

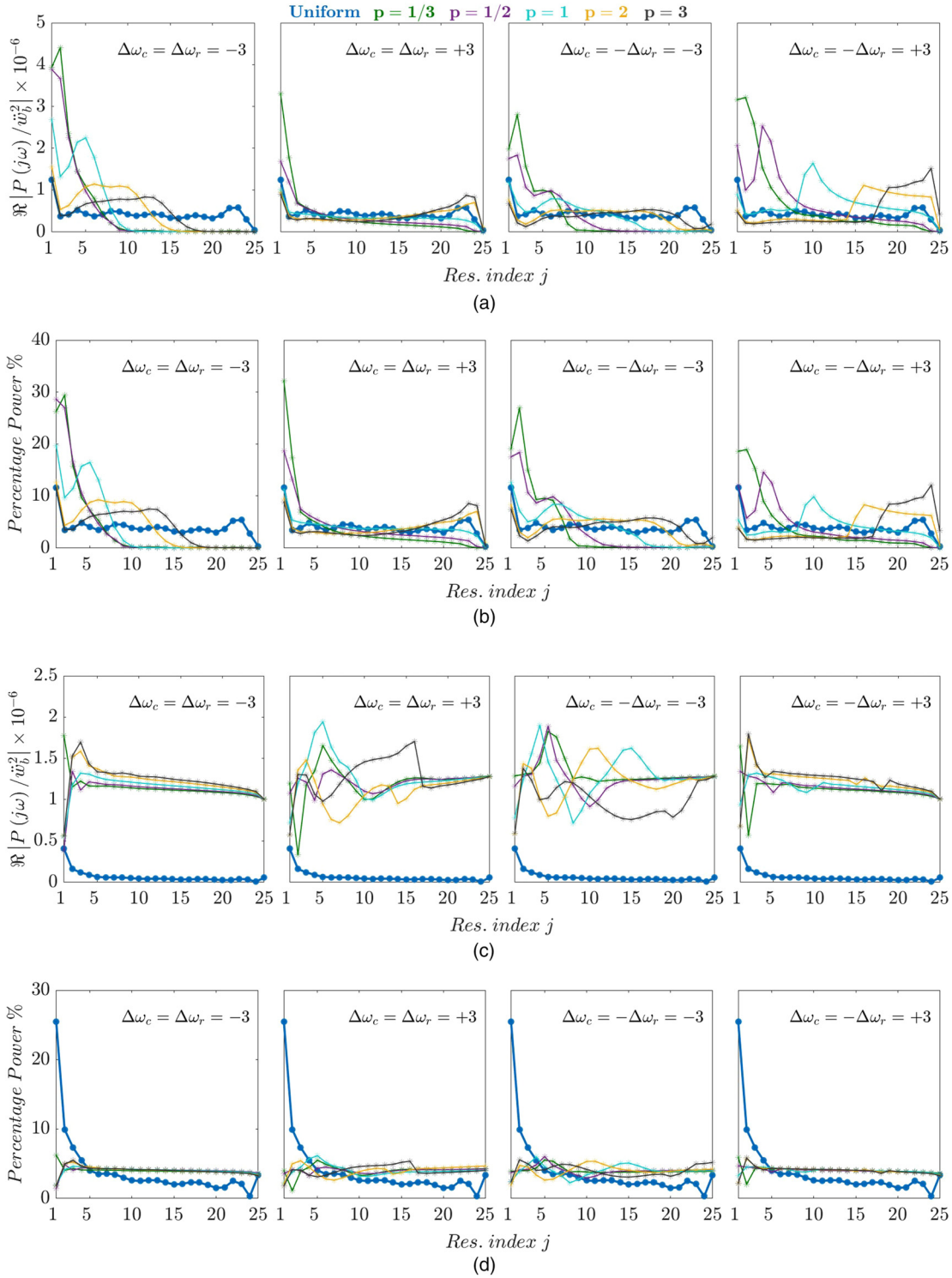

FIG. 12. Real part of the average and percentage power response integrated within $\omega/\omega_1 \in [30-40]$ and upon varying the resonator index j for a graded hybrid metastructure. (a) Average and (b) percentage power fed in the electromechanical resonators. (c) Average and (d) percentage power fed in the mechanical resonators.

IV. CONCLUSIONS

We have analyzed the energy harvesting and attenuation capabilities of hybrid metastructures characterized by different grading laws. In the context of vibration control, such systems are capable of improved dynamic performance as compared to ungraded configurations, both in terms of bandwidth and transmissibility. More specifically, we have observed the presence of grading-induced localized modes that are typical of the rainbow effect and reflect into both power output increase and bandwidth enhancement, which can be relevant for the implementation of energy harvesting devices. Although distinct grading laws can be tailored to provide different spatial localization characteristics and attenuation regions, the improvement in terms of average power output is similar among the configurations analyzed in the paper. Indeed, a careful analysis of the individual resonators has revealed a more regular distribution of the power in space, which justifies the improved performance of graded configurations as compared to the uniform scenarios, where the harvested power is limited within a narrow region and suddenly drops after the first unit cells. Also, our work explores the coexistence of multiple functionalities in a single metastructure, which is not common in the field of mechanics.

AUTHOR DECLARATIONS

Conflict of Interest

The authors have no conflicts to disclose.

Author Contributions

Jonatha Santini: Conceptualization (equal); Formal analysis (lead); Investigation (equal); Methodology (equal); Writing – original draft (equal); Writing – review and editing (equal). **Christopher Sugino:** Conceptualization (equal); Formal analysis (equal); Investigation (equal); Supervision (equal); Writing – original draft (equal); Writing – review and editing (equal). **Emanuele Riva:** Conceptualization (equal); Formal analysis (equal); Investigation (equal); Supervision (equal); Writing – original draft (lead); Writing – review and editing (equal). **Alper Erturk:** Conceptualization (equal); Formal analysis (equal); Investigation (equal); Methodology (equal); Supervision (equal); Writing – original draft (equal); Writing – review and editing (equal).

DATA AVAILABILITY

Data sharing is not applicable to this article as no new data were created or analyzed in this study.

REFERENCES

[1]Z. Liu, X. Zhang, Y. Mao, Y. Zhu, Z. Yang, C. T. Chan, and P. Sheng, "Locally resonant sonic materials," Science **289**(5485), 1734–1736 (2000).
[2]P. Sheng, J. Mei, Z. Liu, and W. Wen, "Dynamic mass density and acoustic metamaterials," Physica B **394**(2), 256–261 (2007).
[3]H. B. Al Ba'ba'a and M. Nouh, "Mechanics of longitudinal and flexural locally resonant elastic metamaterials using a structural power flow approach," Int. J. Mech. Sci. **122**, 341–354 (2017).
[4]C. Sugino, Y. Xia, S. Leadenham, M. Ruzzene, and A. Erturk, "A general theory for bandgap estimation in locally resonant metastructures," J. Sound Vib. **406**, 104–123 (2017).
[5]N. Fang, D. Xi, J. Xu, M. Ambati, W. Srituravanich, C. Sun, and X. Zhang, "Ultrasonic metamaterials with negative modulus," Nat. Mater. **5**(6), 452–456 (2006).
[6]C. Sugino, S. Leadenham, M. Ruzzene, and A. Erturk, "An investigation of electroelastic bandgap formation in locally resonant piezoelectric metastructures," Smart Mater. Struct. **26**(5), 055029 (2017).
[7]V. Romero-García, G. Theocharis, O. Richoux, A. Merkel, V. Tournat, and V. Pagneux, "Perfect and broadband acoustic absorption by critically coupled sub-wavelength resonators," Sci. Rep. **6**(1), 1–8 (2016).
[8]M. Oudich, M. Senesi, M. B. Assouar, M. Ruzenne, J.-H. Sun, B. Vincent, Z. Hou, and T.-T. Wu, "Experimental evidence of locally resonant sonic band gap in two-dimensional phononic stubbed plates," Phys. Rev. B **84**(16), 165136 (2011).
[9]J. Cha, K. W. Kim, and C. Daraio, "Experimental realization of on-chip topological nanoelectromechanical metamaterials," Nature **564**(7735), 229–233 (2018).
[10]J. Cha and C. Daraio, "Electrical tuning of elastic wave propagation in nanomechanical lattices at MHz frequencies," Nat. Nanotechnol. **13**(11), 1016–1020 (2018).
[11]J. Zhu, J. Christensen, J. Jung, L. Martin-Moreno, X. Yin, L. Fok, X. Zhang, and F. Garcia-Vidal, "A holey-structured metamaterial for acoustic deep-subwavelength imaging," Nat. Phys. **7**(1), 52–55 (2011).
[12]A. Colombi, V. Ageeva, R. J. Smith, A. Clare, R. Patel, M. Clark, D. Colquitt, P. Roux, S. Guenneau, and R. V. Craster, "Enhanced sensing and conversion of ultrasonic Rayleigh waves by elastic metasurfaces," Sci. Rep. **7**(1), 1–9 (2017).
[13]J. Marconi, E. Riva, M. Di Ronco, G. Cazzulani, F. Braghin, and M. Ruzzene, "Experimental observation of nonreciprocal band gaps in a space-time-modulated beam using a shunted piezoelectric array," Phys. Rev. Appl. **13**(3), 031001 (2020).
[14]C. Sugino, M. Ruzzene, and A. Erturk, "An analytical framework for locally resonant piezoelectric metamaterial plates," Int. J. Solids Struct. **182-183**, 281–294 (2020).
[15]C. Sugino, M. Ruzzene, and A. Erturk, "Nonreciprocal piezoelectric metamaterial framework and circuit strategies," Phys. Rev. B **102**(1), 014304 (2020).
[16]G. Trainiti, Y. Xia, J. Marconi, G. Cazzulani, A. Erturk, and M. Ruzzene, "Time-periodic stiffness modulation in elastic metamaterials for selective wave filtering: Theory and experiment," Phys. Rev. Lett. **122**(12), 124301 (2019).
[17]C. Sugino, M. Ruzzene, and A. Erturk, "Digitally programmable resonant elastic metamaterials," Phys. Rev. Appl. **13**(6), 061001 (2020).
[18]Y. Xia, E. Riva, M. I. Rosa, G. Cazzulani, A. Erturk, F. Braghin, and M. Ruzzene, "Experimental observation of temporal pumping in electromechanical waveguides," Phys. Rev. Lett. **126**(9), 095501 (2021).
[19]A. Erturk and D. J. Inman, *Piezoelectric Energy Harvesting* (John Wiley & Sons, 2011).
[20]C. Sugino and A. Erturk, "Analysis of multifunctional piezoelectric metastructures for low-frequency bandgap formation and energy harvesting," J. Phys. D: Appl. Phys. **51**(21), 215103 (2018).
[21]K. L. Tsakmakidis, A. D. Boardman, and O. Hess, "'Trapped rainbow' storage of light in metamaterials," Nature **450**(7168), 397–401 (2007).
[22]Q. Gan, Y. Gao, K. Wagner, D. Vezenov, Y. J. Ding, and F. J. Bartoli, "Experimental verification of the rainbow trapping effect in adiabatic plasmonic gratings," Proc. Natl. Acad. Sci. U.S.A. **108**(13), 5169–5173 (2011).
[23]J. Zhu, Y. Chen, X. Zhu, F. J. Garcia-Vidal, X. Yin, W. Zhang, and X. Zhang, "Acoustic rainbow trapping," Sci. Rep. **3**(1), 1–6 (2013).
[24]M. Alshaqaq and A. Erturk, "Graded multifunctional piezoelectric metastructures for wideband vibration attenuation and energy harvesting," Smart Mater. Struct. **30**(1), 015029 (2021).

[25]J. M. De Ponti, L. Iorio, E. Riva, R. Ardito, F. Braghin, and A. Corigliano, "Selective mode conversion and rainbow trapping via graded elastic waveguides," Phys. Rev. Appl. **16**, 034028 (2021).
[26]J. M. De Ponti, A. Colombi, E. Riva, R. Ardito, F. Braghin, A. Corigliano, and R. V. Craster, "Experimental investigation of amplification, via a mechanical delay-line, in a rainbow-based metamaterial for energy harvesting," Appl. Phys. Lett. **117**(14), 143902 (2020).
[27]M. Carrara, M. Cacan, J. Toussaint, M. Leamy, M. Ruzzene, and A. Erturk, "Metamaterial-inspired structures and concepts for elastoacoustic wave energy harvesting," Smart Mater. Struct. **22**(6), 065004 (2013).
[28]C. Sugino, M. Ruzzene, and A. Erturk, "Merging mechanical and electromechanical bandgaps in locally resonant metamaterials and metastructures," J. Mech. Phys. Solids **116**, 323–333 (2018).